

PCCP

Accepted Manuscript



This is an *Accepted Manuscript*, which has been through the Royal Society of Chemistry peer review process and has been accepted for publication.

Accepted Manuscripts are published online shortly after acceptance, before technical editing, formatting and proof reading. Using this free service, authors can make their results available to the community, in citable form, before we publish the edited article. We will replace this *Accepted Manuscript* with the edited and formatted *Advance Article* as soon as it is available.

You can find more information about *Accepted Manuscripts* in the [Information for Authors](#).

Please note that technical editing may introduce minor changes to the text and/or graphics, which may alter content. The journal's standard [Terms & Conditions](#) and the [Ethical guidelines](#) still apply. In no event shall the Royal Society of Chemistry be held responsible for any errors or omissions in this *Accepted Manuscript* or any consequences arising from the use of any information it contains.

The Modification of Ferroelectric LiNbO₃ (0001) Surfaces Using Chromium Oxide Thin Films

M.W. Herdiech^{1,2}, X. Zhu^{1,2}, M.D. Morales-Acosta^{1,3}, F.J. Walker^{1,3}, and E.I. Altman^{1,2,*}

¹*Center for Research on Interface Structures and Phenomena*

²*Department of Chemical and Environmental Engineering*

³*Department of Applied Physics*

Yale University

New Haven, CT 06520

Abstract

The impact of ferroelectric polarization on the chemical and electronic properties of atomically thin layers of non-polar chromium oxide deposited on positively and negatively poled LiNbO₃ (0001) was studied. Chromium (III) oxide readily forms on LiNbO₃; however, annealing at high temperatures was required to maintain well-ordered films as the thickness increased. Prolonged heating at these temperatures caused Cr diffusion into the LiNbO₃ substrate. Comparing Cr 2p x-ray photoelectron spectroscopy (XPS) peak positions as a function of temperature and substrate polarization revealed no evidence of shifts from the peak positions expected for Cr₂O₃. The lack of any band offset between Cr₂O₃ on the oppositely poled surface suggests that charge compensation of the ferroelectric substrate occurs at least predominantly at the surface of the film, as opposed to the film-substrate interface. No evidence of shifts due to oxidation or reduction of the Cr was observed indicating that charge compensation did not involve a change in the ionic state of the Cr. Exposing the films to reactive oxygen species emitted from an oxygen plasma, however, caused a distinct high binding energy shoulder on the Cr 2p_{3/2} XPS peaks that could be associated with oxygen adsorption on surface Cr and concomitant oxidation to Cr⁵⁺. This feature was used to gauge the concentration of O adatoms on the surfaces as a function of temperature for oppositely poled substrates; these measurements did not reveal any significant polarization dependence for oxygen desorption. Further, temperature programmed desorption measurements for a Cr₂O₃ film on α -Al₂O₃ showed a similar trend in O₂ desorption. Therefore, it is concluded that the reactivity of Cr₂O₃ toward O is at least largely independent of substrate polarization despite data suggestive of charge compensation at the film surfaces.

1. Introduction

Much recent work with ferroelectric materials has focused on the surface structure¹⁻⁴ and reactivity⁵⁻¹² of oppositely poled surfaces. Because the surface charge compensation mechanisms that prevent the electrostatic surface energy from diverging must depend on the polarization direction,¹³ oppositely poled surfaces are expected to display different surface properties.¹⁴⁻¹⁶ Since the direction of polar domains in a ferroelectric material can be switched by application of an external electric field, one can envision a class of materials with switchable surface properties. A surface property that could potentially be tuned is reactivity, making way for catalysts whose reactivity and/or selectivity could be altered by application of an external electric field, or by heating above the Curie temperature. Recent studies exploring the reactivity of ferroelectric surfaces toward polar molecules have shown that the heats of adsorption for these molecules are polarization dependent, but that the surfaces tend to be unreactive.^{5,6} Efforts to use ferroelectrics to modify the properties of catalytic metals have yielded ambiguous results. While early experimental studies reported substantial polarization direction dependent reactivity¹⁶ and theory predicted unique reactivity for atomically thin layers on ferroelectric supports,¹⁷ the most recent experimental study found no evidence of the ferroelectric support influencing adsorption on the metal.¹⁸ The lack of any impact was attributed to the metal forming 3D clusters whose surfaces were too far from the ferroelectric interface to be affected by the substrate polarization. Therefore, we seek to create catalytic surfaces with polarization dependent properties by coating ferroelectric substrates with catalytically active oxides that are likely to grow in a layer-by-layer manner; this paper describes the interaction of atomically thin layers of chromium oxide on positively and negatively poled LiNbO₃ (0001) surfaces. It will be shown that ordered, epitaxial Cr₂O₃ thin films can be formed on LiNbO₃. No band offsets between Cr₂O₃ on the oppositely poled surfaces were observed suggesting that charge compensation in the polar system may occur at the Cr₂O₃ surface. Despite the suggestion that the Cr₂O₃ surfaces on oppositely poled LiNbO₃ are distinct, oxygen adsorption strength on the film surfaces was not strongly influenced by the substrate poling direction.

Prior studies involving the reactivity of LiNbO₃ surfaces have shown that while the heats of adsorption of polar molecules are polarization dependent, the surfaces are unreactive.^{5,6} For example, a study by Yun et al. on 2-propanol adsorption on positively and negatively poled LiNbO₃ surfaces found that 2-propanol desorbs from the negatively poled surface 110 K lower

than from the positively poled surface in temperature programmed desorption (TPD) measurements; however, there was no evidence of 2-propanol dissociation.⁵ A study by Garra et al. on water and methanol adsorption on positively and negatively poled LiNbO₃ surfaces found that both molecules desorb from the negatively poled surface at lower temperatures than from the positively poled surface, but the desorption was always molecular.⁶

Despite LiNbO₃'s inertness, its use as a support for catalytically active materials could yield novel reactivity. As even oxides that are generally considered inert can influence the catalytic properties of supported layers,¹⁹ a ferroelectric support may offer the opportunity to modulate catalytic activity since charge compensation of the polar surfaces might include chemical and electronic reconstructions of the active layer. Thus researchers have been motivated to investigate the behavior of metals and metal oxides on LiNbO₃.^{14-16,18,20,21} Inoue et al. studied the activity of Cu on LiNbO₃ for the partial oxidation of methanol to formaldehyde; Cu on the negatively poled surface was found to be more active.¹⁴ The same group also reported a reduced activation energy for CO oxidation on NiO when the NiO was supported on negatively poled LiNbO₃; a curious aspect of these results was that the effects were reported to extend to films as thick as 32 nm.¹⁵ There have also been a series of studies focused on Pd on LiNbO₃.^{16,18,20,21} Initial studies reported a 30 kJ/mol reduction in the activation energy for CO oxidation for 0.02 nm Pd thin films on positively poled LiNbO₃ compared to thicker Pd films on positively poled LiNbO₃ and any Pd thickness on negatively poled LiNbO₃. The lower activation energy was attributed to a weaker Pd–CO bond due to an electron deficiency at the Pd surface caused by attraction of electrons in the metal to the positively poled ferroelectric surface.¹⁶ Similar effects were predicted theoretically for 1-3 atom thick Pt layers on PbTiO₃.¹⁷ Recent experimental work, however, found no evidence that CO adsorption on Pd supported on LiNbO₃ could be influenced by ferroelectric polarization.¹⁸ The lack of any effect was consistent with the observation of 3D cluster growth starting at the lowest coverages.¹⁸ As a result, it was concluded that the Pd surface was too far from the LiNbO₃ surface to be influenced by its polarization. Other recent experimental work supported by theory suggested that Pd could be made to grow layer-by-layer on negatively poled LiNbO₃ but not on positively poled LiNbO₃.²⁰ Still, a reduced activation energy for CO oxidation on the thinnest Pd layers on positively poled LiNbO₃ cannot be reconciled with this finding. The limited thickness over which a ferroelectric can influence a metal, coupled with the high surface energies of metals that make them susceptible to 3D

clustering on oxide surfaces, therefore, creates substantial hurdles to realizing switchable catalysts based on ferroelectric-supported metals. We therefore turn our attention to modulating the activity of catalytically active oxide layers that can be stable as 2D films and where the influence of the ferroelectric is suggested to extend well beyond a monolayer.¹⁵

The present study focuses on chromium oxide for activating LiNbO₃ surfaces. Chromium oxide was chosen because of its importance as a catalytic material and its structural similarity to LiNbO₃ which suggests that it should be possible to form epitaxial chromium oxide layers. Chromium oxide-based catalysts have been well-studied and are catalytically active for a variety of reactions; industrial applications of these catalysts include ethylene polymerization,²²⁻²⁴ alkane dehydrogenation,²⁵ and the selective oxidation of alcohols.²⁶ Chromium (III) oxide adopts the corundum structure, while LiNbO₃ crystallizes in a similar structure, except with Li⁺ and Nb⁵⁺ substituting for Cr³⁺.²⁷⁻²⁹ Below the 1470 K Curie temperature,²⁷ the LiNbO₃ crystal can be envisioned as alternating planes of Li, O₃, and Nb in the [0001] direction. Because the charge on the Nb planes is greater than that on the Li planes, a dipole can be associated with the Li-O₃-Nb repeat unit accounting for the polarization. The lattice mismatch between Cr₂O₃ and LiNbO₃ is only 3.6%. Therefore, as illustrated in Fig. 1, when Cr₂O₃ is grown on LiNbO₃ (0001) the oxygen sublattice can continue unabated and Cr can fill the cation sites in the same order as the substrate. Figure 1 is based on the bulk structures and does not include reconstructions at the interface that compensate the bulk polarization of bare LiNbO₃ surfaces.¹⁻³ For the heteroepitaxial system, assuming that the charge compensation layer does not migrate to beneath the LiNbO₃ surface, several charge compensation scenarios involving the film-substrate interface and film surface can be envisioned, including: 1) retention of the LiNbO₃ surface reconstructions; 2) new interfacial reconstructions; 3) change in the Cr oxidation state at the interface; and 4) migration of the charge compensation layer to the Cr₂O₃ surface where reconstructions or changes in the surface Cr oxidation state may be induced. Each scenario entails a unique x-ray photoelectron spectroscopy (XPS) signature and a different mechanism for modifying the reactivity of the Cr₂O₃ oxide. For example, reconstructions at the interface would yield dipoles across the Cr₂O₃/LiNbO₃ interface that would create opposite band offsets for Cr₂O₃ on oppositely poled surfaces. Meanwhile, a change in oxidation state of the Cr at the interface would yield XPS peak shifts that decay with the thickness of the Cr₂O₃ layer, while migration of the charge compensation layer to the Cr₂O₃ surface where it may induce a surface

reconstruction would have minimal effect on the XPS spectra. The expectation is that charge compensation at the interface would only impact the reactivity of the first Cr_2O_3 layers either through structural modification of the surface or change of the Cr oxidation state. In contrast charge compensation at the Cr_2O_3 surface would yield structures or electronic states not seen at the surface of bulk, non-polar Cr_2O_3 (0001), even as the film thickness increases.

In this paper it is shown that ordered Cr_2O_3 films can be grown on both positively and negatively poled LiNbO_3 as evidenced by XPS, low-energy electron diffraction (LEED), and x-ray diffraction (XRD) measurements. The high temperatures required for epitaxial growth, however, can cause Cr diffusion into LiNbO_3 thereby possibly blurring the $\text{Cr}_2\text{O}_3/\text{LiNbO}_3$ interface. No evidence of band offsets due to interfacial dipoles or shifts in the Cr XPS peak positions that could be associated with interfacial Cr oxidation or reduction could be detected, suggesting that the charge compensation layer for the polar system moves to the film surface. It will be shown that LiNbO_3 supported Cr_2O_3 is active for oxygen adsorption but the oxygen adsorption strength is not strongly influenced by the ferroelectric support.

2. Experimental

Experiments were carried out using two ultra-high vacuum (UHV) systems, both of which have been described in detail previously.^{12,30} Briefly, the first is an interconnected three-chamber system with separate growth, analysis, and microscopy chambers; in this study only the former two chambers were used. The turbo-pumped growth chamber is equipped with effusion cells and electron beam evaporators; Cr was deposited using one of the electron beam evaporators. Additionally, there is a microwave electron cyclotron resonance (ECR) plasma source for generating atomic oxygen, a differentially pumped 20 keV electron gun for reflection high-energy electron diffraction (RHEED) measurements, and quartz crystal oscillators (QCOs) for measuring deposition rates. The ion-pumped analysis chamber is equipped with a double pass cylindrical mirror analyzer (DP-CMA), a dual anode x-ray source for XPS, and rear-view LEED optics. The typical base pressure is 1×10^{-9} Torr in the growth chamber and 3×10^{-10} Torr in the analysis chamber. Samples were mounted on transferable sample holders with a chromel-alumel thermocouple mounted to the baseplate behind the sample and were radiatively heated from a filament behind the sample baseplate.

The second system is a single chamber system equipped with a differentially pumped microwave ECR plasma source, a differentially pumped quadrupole mass spectrometer, gas dosers, rear-view LEED optics, a dual-anode x-ray source, an ion gun, a Kelvin probe, a hemispherical energy analyzer, a QCO, and several resistively heated tungsten wire baskets for depositing various metals, Cr in these experiments. The system has a typical base pressure of 3×10^{-10} Torr. The ion-pumped main chamber is connected to a turbo-pumped side chamber used for introducing samples and for differential pumping of the plasma source. Samples were mounted on transferable sample holders that incorporated thermocouple contacts and a heater. In this system the thermocouple was attached to the front surface of the crystals using a high temperature ceramic adhesive.¹ Both UHV systems were used for film growth, LEED, and XPS. The three-chamber system was used for RHEED measurements and the single chamber system for TPD experiments. X-ray diffraction (XRD) and x-ray reflectivity (XRR) measurements were performed *ex-situ* with a Rigaku SmartLab x-ray diffractometer with a two crystal Ge (220) monochromator on the incident beam and Cu K_{α} radiation, operated at 45 kV and 200 mA.

The different thermocouple placement in the two systems can lead to discrepancies in the temperature measurements with the thermocouple on the backing plate possibly overestimating the surface temperature. Calculation of the thermal gradient across the sample based on thermal conduction and radiative losses from the surface suggest a temperature difference between the backing plate and surface of less than 3 K across the temperature range of interest. This estimate assumes perfect thermal contact between the sample and the backing plate; nonetheless, it will be shown that the oxygen desorption temperature determined by XPS with the thermocouple on the backing plate agrees with the TPD peak temperature measured with the thermocouple glued to the surface.

The XPS spectra were obtained using 1486.61 eV non-monochromatic Al K_{α} radiation. Because charging of the insulating substrate tended to shift the kinetic energy of the XPS peaks, the binding energies were referenced by positioning the Nb $3d_{5/2}$ peaks at a binding energy of $207.2 \pm .001$ eV as discussed previously.¹⁸ Finally, because LiNbO_3 is pyroelectric, its surface potential changes with temperature which can cause the positions of XPS peaks to drift.¹⁸ Therefore, it was necessary to stabilize the temperature before performing the measurements. The XPS peak locations were obtained by fitting the data to mixed Gaussian-Lorentzian peak shapes. All LEED patterns were collected at room temperature except for the pattern shown in

Fig. 6c, which was collected at 575 K since charging effects distorted the image at lower temperatures.

Sapphire and nearly stoichiometric (49.8 mol% Li_2O) LiNbO_3 samples were obtained from MTI Corporation. The samples were polished on one side and oriented within $\pm 0.5^\circ$ of (0001). The polarization direction of LiNbO_3 could be determined and switched following methods described previously.¹ Prior to insertion into the UHV system, LiNbO_3 samples were annealed in flowing air at 1075 K for 10-15 hours,¹⁸ and $\alpha\text{-Al}_2\text{O}_3$ samples were annealed in flowing air for an hour at 875 K.³¹ Once in the UHV system, both $\alpha\text{-Al}_2\text{O}_3$ and LiNbO_3 samples were cleaned in the plume of the oxygen plasma at 575 K for up to an hour to get rid of impurities, mainly C. Chromium pieces (99.997%) for deposition were obtained from Alfa Aesar.

Chromium oxide films were grown between 575 – 725 K in background O_2 pressures between 5×10^{-6} – 1×10^{-5} Torr. Although prior work on $\alpha\text{-Al}_2\text{O}_3$ (0001) (compressive mismatch of 3.6% compared to the 3.6% tensile mismatch with LiNbO_3) showed that high quality epitaxial Cr_2O_3 , as evidenced by RHEED oscillations, could be grown by oxygen plasma assisted molecular beam epitaxy at 775 K, we found that the plasma was not necessary to form Cr_2O_3 over the temperature range studied. Because more oxidized Cr oxides may form at lower temperatures³² and, as described below, atomic oxygen from the plasma can adsorb on Cr_2O_3 up to high temperatures, we did not grow the films in the plasma.^{33,34} For LiNbO_3 , lower growth temperatures are desirable since it can start to lose Li_2O in UHV at temperatures as low as 500 K.¹ For thinner films where we monitored the evolution of the properties as a function of coverage, the thickness is provided in units of monolayers where 1 ML is taken as the distance between Cr planes along [0001] in Cr_2O_3 , 0.227 nm; for thicker films expected to display bulk-like properties the thickness is given in nm with the rough number of corresponding monolayers provided in parentheses.

3. Results

3.1 Evolution of Film Structure During Growth and Annealing

As described above, low temperatures are desired for epitaxial growth on LiNbO_3 in UHV; therefore, we investigated the effect of growth temperature and subsequent annealing in atmospheric pressure oxygen on Cr_2O_3 growth. Growth at 575 K on LiNbO_3 resulted in rapid

attenuation of the LiNbO₃ RHEED pattern for both polarizations and no evidence of order in XRD measurements after 3 ML of Cr₂O₃ was deposited on the positively poled substrate (Fig. 2a), although x-ray reflectivity (XRR; Fig. 2b) measurements indicated a film density consistent with Cr₂O₃.

Analysis of the XRD patterns confirm the presence of (001)-oriented Cr₂O₃, with no evidence for other orientations or phases in the film. As the film was annealed to progressively higher temperatures, a distinct (006) Cr₂O₃ diffraction peak began to take shape by 775 K and increased in intensity as the temperature was raised to 975 K as shown by the XRD peak profiles extracted from the measured reciprocal space maps in Fig. 2a. The XRR fringes in Fig. 2b for the film annealed at 875 K suggest a roughness at the interface between the Cr₂O₃ and LiNbO₃ of 0.21 nm, or close to the thickness of one atomic layer of both Cr₂O₃ (0.227 nm) and LiNbO₃ (0.231 nm), for the as-grown film and 0.35 nm after annealing at 875 K for 30 min. The increased interfacial roughness is likely the result of diffusion of some of the film into the bulk substrate. Chromium diffusion is further supported by another component of the XRR data: the slight decrease in the peak spacings indicate that the Cr₂O₃ film became 4 Å thinner after annealing. Based on the XRD results, the growth temperature for the remaining experiments was set at 725 K, below the temperature where LiNbO₃ can be damaged significantly in UHV yet high enough to yield evidence of order in XRD, and the annealing temperature to 875 K which yields a distinct Cr₂O₃ XRD peak. As will be detailed below, higher annealing temperatures were avoided to reduce Cr migration into the bulk.

To determine if Cr₂O₃ forms two dimensional layers on LiNbO₃ at 725 K, series of XPS measurements were performed after incremental Cr₂O₃ deposition; the results are provided in Figs. 3a and 3b for the positively and negatively poled surfaces, respectively. Because the oxygen density is largely constant across the Cr₂O₃/LiNbO₃ interface, the normalized Cr peak intensity is taken as the Cr 2p/O 1s peak area ratio divided by that same ratio for a 20 nm (≈ 90 ML) thick film while the Nb peak intensity is taken as the Nb 3d/O 1s peak area ratio divided by that same ratio for the bare LiNbO₃ surface. In Fig. 3, the growth of the Cr 2p peaks and attenuation of the Nb 3d peaks are compared to expectations for layer-by-layer growth calculated considering the Beer-Lambert law³⁵ and electron mean free paths derived from the universal curve for mean free paths.³⁶ Figure 3 shows good agreement between the calculated and experimental results for both LiNbO₃ surfaces, indicating that Cr₂O₃ wets the LiNbO₃ surfaces.

Growth at 725 K initially yielded high quality surfaces as evidenced by RHEED and LEED. As shown in Fig. 4 for the negatively poled surface, the RHEED pattern for the first couple of monolayers was similar to that of the substrate, but thereafter attenuated and was difficult to detect by 6 ML. The LEED data in Fig. 5 tell a similar story: the pattern at 1 ML (Fig. 5a) is sharp with a low background; the background at 8.6 ML is much higher (Fig. 5b); and by 10 ML (Fig. 5c) only a few diffuse spots could be detected. When comparing the patterns in Fig. 5, note that each pattern was recorded at the energy that yielded the most intense pattern, thus the changes from Fig. 5a to 5c reflect a deterioration of the surface order. Also note that the retention of the LEED pattern to higher coverages may reflect slight differences in the growth process for the RHEED and LEED experiments: the RHEED patterns were recorded during continuous growth, while the growth had to be stopped and restarted to record the LEED data; before restarting, the sample was heated at the growth temperature in the plume of the oxygen plasma to remove any impurities that may have accumulated after stopping the growth and analyzing the sample. Because the data in Fig. 3 suggests that Cr_2O_3 wets the LiNbO_3 surface, the deterioration of the RHEED and LEED patterns cannot be explained by a gradual covering of the LiNbO_3 surfaces, rather the order of the Cr_2O_3 film must be deteriorating. While epitaxial Cr_2O_3 growth on LiNbO_3 polar surfaces at 725 K was limited to the first few layers, annealing thicker films in air at 875 K produced well-ordered surfaces as anticipated from the XRD data in Fig. 2a. As shown in Figs. 6a-c, the expected hexagonal LEED patterns were obtained after annealing 12 nm (≈ 55 ML) Cr_2O_3 thick on $\alpha\text{-Al}_2\text{O}_3$ (0001) (Fig. 6a) and 20 nm (≈ 90 ML) thick Cr_2O_3 films on positively (Fig. 6b) and negatively (Fig. 6c) poled LiNbO_3 (0001).

Although annealing in air promoted epitaxial crystallization of the Cr_2O_3 films, prolonged annealing also caused significant Cr diffusion into the LiNbO_3 substrate independent of polarization direction. As illustrated in Fig. 7 for a 10.0 ML Cr_2O_3 film on positively poled LiNbO_3 , after annealing in air at 875 K for 12 h the intensity of the Cr 2p peaks was reduced by a factor of 2.3, while the intensity of the substrate Nb 3d peaks increased by a factor of 2.9. Chromium diffusion into LiNbO_3 following metallic Cr deposition and annealing in air has previously been observed at much higher temperatures, above 1200 K.³⁷ Chromium prefers to substitute for Li^+ in the lattice but can also fill intrinsic vacant octahedral sites in the structure.³⁸ Two factors can contribute to the much lower diffusion temperatures seen here. First, diffusion of metallic Cr layers can be limited by the rate of oxidation of the metallic Cr to Cr^{3+} . Second, it

has been shown that heating LiNbO₃ (0001) surfaces in UHV causes Li₂O desorption beginning at 500 K which creates Li vacancies in the surface region that can be filled by Cr³⁺.¹ During annealing in air Cr³⁺/Li⁺ exchange and Li₂O desorption may occur continuously, leading to Cr³⁺ diffusing deep into the bulk and beyond the XPS detection range.

3.2 Investigation of Charge Compensation Mechanisms

As described in the Introduction, comparison of the Cr XPS peaks for Cr₂O₃ on oppositely poled LiNbO₃ surfaces can be a sensitive probe of the charge compensation mechanism of the polar system. Figure 8 illustrates this comparison for a series of coverages. For both positively and negatively poled substrates, the binding energies of the Cr 2p_{1/2} and Cr 2p_{3/2} peaks are 586.7 and 576.9 eV, respectively, independent of coverage. These positions indicate that the chromium is at least predominantly Cr³⁺, or in the form of Cr₂O₃, the most stable form of chromium oxide over a wide range of conditions.³⁹ For Cr₂O₃, literature values for the Cr 2p_{3/2} peak range from 576.7 – 576.8 eV while the Cr 2p_{1/2} peak appears between 586.4 – 586.7 eV.⁴⁰⁻⁴² While the peak positions observed here are at the upper ends of these ranges, other stable oxidation states of Cr can be ruled out. For CrO₃, the Cr 2p_{3/2} peak position is more than 1.5 eV higher at 578.3 eV.⁴¹ Meanwhile, Cr⁴⁺ is unique in that its XPS peaks are at lower binding energies than those of Cr³⁺ despite the higher oxidation state; reported Cr 2p_{3/2} peak positions for CrO₂ range from 576.3 – 576.4 eV.^{40,41} More reduced Cr²⁺ is relatively unstable; it readily oxidizes to Cr³⁺, and is thus not expected to form under the conditions employed here. Lastly, XPS peaks for Cr metal are at significantly lower binding energies than those for oxidized Cr,⁴³ so Cr⁰ can be ruled out as well. It should be noted that the O 1s peak does not attenuate as the Cr oxide film thickened, also consistent with Cr₂O₃ growth. The Cr 2p_{3/2} peaks in Figs. 8a and 8b reveal a high binding energy shoulder for lower coverage, consistent with oxidation of Cr to Cr⁵⁺ or Cr⁶⁺.^{44,45} It will be shown below that this feature is due to oxygen adsorption and can be removed by flashing to high temperatures.

The lack of any coverage or polarization dependence of the position or shape of the Cr 2p peaks rules out changes in the Cr oxidation state at either the surface or interface as the charge compensation mechanism. For negatively poled LiNbO₃, positive surface charges are necessary to compensate the bulk polarization,¹³ which could be supplied by oxidation of Cr³⁺ to Cr⁴⁺. Meanwhile, the positively poled surface could be passivated by reduction of Cr³⁺ to Cr²⁺. Since

the surface charge density or ferroelectric polarization of LiNbO_3 is 0.8 C/m^2 ,⁴⁶ or $1.15 \text{ e}^-/\text{unit cell}$, and each (0001) surface unit cell of the corundum structure contains two cations in octahedral sites (one above the outermost oxygen plane, the other below it), the field from the substrate could be passivated by approximately half the Cr atoms at the interface or surface changing their oxidation state by ± 1 . As described above, such changes in oxidation state would yield binding energies substantially lower than Cr^{3+} . With roughly 0.5 ML of Cr changing oxidation state to pacify the surface, the expectation would be that a low binding energy peak would appear at low coverages that would gradually attenuate as the Cr oxide film thickened. The data in Fig. 8 show no evidence of this behavior and therefore it is concluded that the charge compensation mechanism does not involve filling or depleting surface or interface electronic states, thereby changing the Cr oxidation state.

Regardless of whether charge compensation occurs through electronic or atomic reconstruction, charge compensation at the $\text{Cr}_2\text{O}_3/\text{LiNbO}_3$ interface would create an interfacial dipole that would lead to a band offset between the Cr_2O_3 film and the LiNbO_3 substrate. Since this band offset would be opposite for negatively and positively poled LiNbO_3 , and because the Cr XPS peaks are referenced to the Nb 3d peaks, interfacial charge compensation should lead to a rigid shift of the Cr oxide XPS peaks independent of coverage for oppositely poled LiNbO_3 substrates. Using the LiNbO_3 bulk polarization of 0.8 C/m^2 and dielectric constant of 27.3,⁴⁷ modeling the charges across the interface as a parallel plate capacitor with a thickness of 0.1 nm (approximately the distance between atomic planes in the [0001] direction of LiNbO_3 ; see Fig. 1a) suggests a 0.33 V potential across the interface which would create a band offset of 0.66 eV between Cr oxide on positively and negatively poled LiNbO_3 . Recently, we showed that BF_3 physisorbed on oppositely poled LiNbO_3 surfaces exhibits a smaller 0.3 eV difference in the F 1s peak position on positively and negatively poled LiNbO_3 due to such electrostatic effects.¹² The data in Fig. 8 reveal no evidence of such a large difference between the Cr 2p peaks on the two LiNbO_3 surfaces.

We also searched for band offsets by recording XPS spectra as a function of temperature. Because LiNbO_3 is pyroelectric, any band offsets due to interfacial dipoles would be expected to change with temperature. In vacuum at modest temperatures where there are no thermally excited carriers within LiNbO_3 , it has been shown that heating LiNbO_3 can generate enormous fields.⁴⁸⁻⁵⁰ For the 0.5 mm thick samples used in this study, the $-40 \mu\text{C/m}^2\text{K}$ pyroelectric

coefficient of LiNbO_3 ⁵¹ suggests a potential as large as 83 V could develop across the sample for just a 1 K temperature change, assuming that the compensating charges at the surface or interface are frozen. While the x-rays used to generate the photoelectrons for XPS measurements can supply mobile carriers to screen this potential, we recently observed a 60 meV shift in the Pb 4f peaks of a 10 nm (\approx 25 ML) thick ferroelectric and pyroelectric lead zirconate titanate (PZT) thin film on SrRuO_3 when the film was heated from room temperature to just above 400 K,¹² a much larger shift would be expected for the 0.5 mm thick LiNbO_3 samples. Figures 9a and 9b show the Cr $2p_{3/2}$ XPS peak positions for 3 ML Cr oxide films on positively and negatively poled LiNbO_3 , respectively, as a function of temperature. In these experiments, the films were heated incrementally from 300 K to 425 K, and then cooled incrementally back to 300 K; the measurements were performed while holding the samples at the temperatures indicated. Figure 9 shows that the peak positions do not change with temperature, with one exception. In going from 300 K to 350 K, and from 350 K to 300 K, the Cr 2p peaks on negatively poled LiNbO_3 show a reversible shift to higher binding energy, by \sim 0.3 eV at 350 K. The shift to higher binding energies with increasing temperature is consistent with the reduced bulk polarization creating excess positive charge at the interface which accelerates electrons emitted from the substrate but not those from the film; since the Nb $3d_{5/2}$ peak is used as a fixed reference, the Cr binding energy would appear to increase. This experiment, however, was repeated for other films of similar thickness on the negatively poled substrate and the shift was not consistently observed (three additional films were studied, one gave similar results, the other two showed no measurable shift with temperature). Several other factors also argue against assigning the observed shift to changes in the magnitude of an interfacial dipole. First, the positive surface would be expected to show an opposite shift which was not seen. In addition, the shift stops at just 350 K. For the experiments on 10 nm (\approx 25 ML) thick PZT mentioned above, a reversal in the trend was observed above 400 K as thermally activated carriers became sufficient to equilibrate the surface charge required to compensate the lower bulk polarization; once the temperature is high enough for the trend to reverse, the interface potential does not return to its original value on cooling as the compensating charges become frozen at the lower value required to compensate the lower bulk polarization at higher temperatures. For LiNbO_3 the conductivity does not become sufficient to equilibrate the surface charge until 475 K⁵² and in Fig. 9b the binding energy returns to its initial value after heating to 425 K, at least 75 K above the

temperature at which the Cr 2p peaks stopped shifting. Finally, the Neel temperature for bulk Cr_2O_3 is 307 K, within the temperature range where the shifts were seen, and this phase transition from antiferromagnetic to paramagnetic could have a small effect on the Cr XPS peaks. For example, using angle-resolved photoelectron spectroscopy Klebanoff et al. observed small shifts in binding energies of surface features for Cr (001) in heating incrementally through several magnetic phase transitions.⁵³ The sensitivity of such phase transitions to the structural order of the material may account for why the shift was not consistently seen.⁵⁴⁻⁵⁷ For these reasons, it is concluded that substantial dipoles do not exist at the $\text{Cr}_2\text{O}_3/\text{LiNbO}_3$ (0001) interface.

3.3 Oxygen Adsorption

As noted above, a weak high binding energy shoulder on the Cr 2p XPS peaks at lower coverages could be seen following growth. Figure 10 shows for three Cr oxide coverages on both the positively and negatively poled LiNbO_3 substrates, that the intensity of this feature could be greatly enhanced by exposing the surfaces to reactive oxygen species emitted by the plasma source at 295 K. The intensity of these features relative to the peaks observed prior to oxygen plasma treatment decreased with increasing Cr oxide coverage, consistent with changes restricted to the surface layer. Prior XPS studies of chromium oxide catalysts on Al_2O_3 and SiO_2 supports have shown that annealing in air produces high binding energy shoulders attributed to Cr^{6+} formation.^{44,45} UV-visible-near infrared diffuse reflectance spectroscopy also provided evidence that supported Cr oxide could be at least partially oxidized to Cr^{6+} by heating at 825 K in O_2 .⁵⁸ In this case, Cr^{6+} could be eliminated by exposing the sample to CO at elevated temperatures and restored by again heating in O_2 . Thus, the changes in the Cr 2p spectra caused by the plasma treatment are consistent with the known behavior of Cr_2O_3 in oxidizing environments.

Exposure to the reactive oxygen species emitted by the plasma source had no effect on the surface structural order; LEED patterns for both as grown thinner films and thicker films annealed in air were (1x1) before and after the plasma treatment (Figs. 11a and 11b). In addition, the submonolayer films in Fig. 10 show a high binding energy feature to low binding energy feature ratio close to 1:1. These data are consistent with O atom adsorption on exposed Cr atoms on the Cr_2O_3 (0001) surface. As illustrated in Fig. 1a, along [0001] Cr_2O_3 is built up by stacking stoichiometric Cr–O₃–Cr trilayers; the non-polar (0001) surface unit cell exposes one Cr atom

above the O₃ plane and a second inaccessible Cr atom below the O₃ plane as shown in Fig. 1b. Thus, capping each exposed Cr atom with oxygen would not change the surface periodicity and, up to 1 ML, would oxidize half of the Cr in Cr₂O₃. In this case, the formation of such a chromyl species on Cr₂O₃ would yield a nominal Cr oxidation state of 5+, consistent with the observed magnitude of the shift to higher binding energy. Previously, York et al. have reported similar capping oxygen species on Cr₂O₃ (10 $\bar{1}$ 2).⁵⁹

To determine how strongly the oxygen is adsorbed to the surface, XPS measurements were performed as a function of temperature; these data are provided in Fig. 12a for 1.6 ML Cr oxide on positively poled LiNbO₃ and in Fig. 12b for 3.1 ML Cr oxide on negatively poled LiNbO₃. The data were collected by slowly heating the samples to the temperatures indicated in the figure and then collecting the spectra at that same temperature. For both films, the high binding energy shoulder on the Cr 2p_{3/2} peak attenuates slightly while heating to 700 K. By ~800 K, approximately half of the high binding energy shoulder is gone. These data show no obvious difference in how strongly the oxygen is adsorbed. To better understand the desorption behavior of the oxygen adatoms as a function of substrate polarization, TPD measurements were attempted. Unfortunately, the decomposition of the LiNbO₃ substrate starting at lower temperatures generated large amounts of Li₂O and O₂ that masked the ability to unambiguously distinguish oxygen desorption from the Cr oxide. Still, Fig. 12c shows for 6.0 ML Cr₂O₃ on positively poled LiNbO₃ that ramping the sample temperature at a rate of 2 K/sec to 925 K and then cooling to room temperature can completely remove the adsorbed oxygen.

To determine if the ferroelectric substrate plays a role in oxygen adsorption on the thin Cr oxide layers on LiNbO₃, similar measurements were performed on epitaxial Cr₂O₃ films grown on α -Al₂O₃ (0001). The *a* lattice constant of α -Al₂O₃ is 0.476 nm compared to 0.496 nm for Cr₂O₃ and 0.515 nm for LiNbO₃ and so the magnitude of the lattice mismatch is similar for α -Al₂O₃ and LiNbO₃ but is compressive for α -Al₂O₃ and tensile for LiNbO₃. Nonetheless, Fig. 12d shows a similar high binding energy shoulder on the Cr 2p_{3/2} XPS peak after exposure of Cr₂O₃/ α -Al₂O₃ to reactive oxygen species emitted by the plasma source near room temperature, and that the shoulder is partially attenuated after heating the sample to 800 K. Without the complication of the support decomposing, we were able to monitor desorption of this adsorbed oxygen on Cr₂O₃/ α -Al₂O₃ with TPD; a result is shown in Fig. 13 for a 12 nm (\approx 55 ML) thick Cr₂O₃ film. The run was terminated before the oxygen signal returned to the baseline because the

temperature reached the maximum of the thermocouple amplifier so that a linear heating rate could not be maintained above this temperature. Figure 13 shows that O₂ desorption begins just after 600 K, with the desorption rate reaching a maximum at 815 K. Figures 12a and 12b show that by 700 K, a small portion of O adatoms have desorbed, and that by close to 800 K, roughly half of the initial high binding energy shoulder has attenuated, thus drawing similarities to the desorption trace in Fig. 13.

4. Discussion

A key question concerning the growth of non-polar Cr₂O₃ on top of the polar LiNbO₃ polar surfaces concerns the fate of the charge compensating layer at the starting surfaces. This question was addressed by monitoring the positions of the Cr 2p XPS peaks relative to the Nb 3d peaks as a function of coverage, temperature, and substrate polarization direction. The resulting spectra revealed no significant deviations from the peak position expected for Cr³⁺ independent of coverage, temperature, and poling direction. Returning to the four charge compensation scenarios laid out in the Introduction, these results eliminate retention of the bare LiNbO₃ surface reconstructions as well as new interfacial reconstructions, both of which would lead to band offsets between positively and negatively poled substrates. We can also eliminate any mechanism involving changes in the Cr oxidation state, either at the interface or at the Cr₂O₃ surface. This suggests that the charge compensation layer migrates to the Cr₂O₃ surface and, further, that charge compensation impacts oxygen rather than Cr, through, for example, formation of charged oxygen vacancies on the negative surface which would supply positive charge and oxygen anion adsorption on the positive surface which would supply negative charge. Since Cr is observed to diffuse into LiNbO₃, however, charge compensation mechanisms involving Cr interstitials and Cr substitution for Li or Nb must also be considered. At the negative interface, either interstitial Cr³⁺ or Cr⁵⁺ substituting for Li⁺ would supply positive compensating charges, while at the positive interface Cr³⁺ substituting for Nb⁵⁺ would yield negative compensating charges. If this substitution were restricted to the interface, then band offsets between positively and negatively poled substrates would still be seen, which was not the case. Further, the Cr³⁺ substitution for Nb⁵⁺ required to compensate the positive surface has not been seen on LiNbO₃.³⁸ Alternatively, Cr³⁺ intermixed with Li⁺ and Nb⁵⁺ over a wider region may also be possible. If this region was up to the ≈ 3 nm sampling depth of XPS, this would lead

to oppositely asymmetric broadening of the XPS peaks for the positively and negatively poled substrates, which was not seen. Another possibility that could explain the XPS results is that charge compensation in the Cr_2O_3 - LiNbO_3 system occurs beneath the LiNbO_3 surface, beyond the XPS sampling depth; however, the mechanism by which this would occur is unclear. Further, since bare LiNbO_3 undergoes reconstructions at the surface to cancel the thickness dependent dipole¹⁻³, it is unlikely that the addition of the Cr_2O_3 film would drive the existing charge compensating layer deep into the LiNbO_3 substrate. Thus, the data together with the literature suggest that the charge compensation layer migrates to the Cr_2O_3 surface where it impacts oxygen rather than Cr; however, it should be noted that no significant change in the O 1s XPS peak shape or position as a function of temperature, substrate polarization, or Cr_2O_3 film thickness was observed.

The above arguments all assume an abrupt charge compensation region. Photoelectron emission microscopy of periodically poled LiNbO_3 surfaces support an abrupt charge compensation layer at bare LiNbO_3 surfaces,⁶⁰ consistent with experimental observations^{1,3} of chemical reconstructions at the surface that can compensate the polarization as well as expectations for wide band gap materials such as LiNbO_3 . Since Cr migrates into bulk LiNbO_3 , a thicker charge compensation region must be considered for $\text{Cr}_2\text{O}_3/\text{LiNbO}_3$. Such thick charge compensation regions typically occur in polar materials with band gaps small enough to allow mobile carriers in the bulk to fill or deplete regions over thousands of Ångstroms on both sides of a polar crystal.⁶¹ Because charge compensation would occur gradually over a region much thicker than the XPS sampling depth, peak shifts between oppositely poled surfaces would not be observed.

The observed oxidation of surface Cr in highly oxidizing environments allowed a first look at how the substrate polarization affects the reactivity of thin Cr_2O_3 layers. Because LiNbO_3 decomposition in vacuum obscured oxygen desorption from the Cr_2O_3 layer, TPD measurements quantifying the oxygen adsorption strength were not possible. Instead, more granular temperature dependent XPS measurements followed the attenuation of the high binding energy shoulder of the Cr $2p_{3/2}$ peak associated with adsorbed oxygen. These measurements showed little polarization dependence. Moreover, similar oxygen adsorption was seen on comparatively thick Cr_2O_3 (0001) on non-polar $\alpha\text{-Al}_2\text{O}_3$ which yielded O_2 TPD curves consistent with the

temperature dependent XPS measurements for $\text{Cr}_2\text{O}_3/\text{LiNbO}_3$. Thus, at least for oxygen adsorption, the ferroelectric polarization direction does not strongly impact the Cr_2O_3 .

It was suggested above that adsorbed oxygen anions and charged oxygen vacancies could supply the necessary compensating charges to stabilize the positively and negatively poled $\text{Cr}_2\text{O}_3/\text{LiNbO}_3$ systems, respectively. It is important to distinguish the adsorbed oxygen probed by oxygen plasma treatment and temperature dependent XPS measurements from surface species that stabilize the polar system and cannot be removed without changing the surface atomic electronic structure to maintain charge compensation or bulk restructuring to eliminate the polarization. Because there is no apparent polarization dependence on the capping O that adsorbs after exposure to oxygen plasma, this furthers the conclusion that surface Cr does not play a significant role in the charge compensation mechanism in the system.

5. Conclusions

Well-ordered Cr_2O_3 films can be fabricated on positively and negatively poled LiNbO_3 ; however, the conditions necessary to produce the films can cause Cr diffusion into the LiNbO_3 . The lack of any band offset between Cr_2O_3 films on oppositely poled LiNbO_3 surfaces indicates that charge compensation does not occur abruptly at the interface between LiNbO_3 and the Cr_2O_3 film, rather the results suggest that the charge compensation layer that stabilizes the polar material occurs at the film surface. It was also shown that surface Cr in the Cr_2O_3 film can be oxidized to Cr^{5+} by atomic oxygen. Despite the suggestion that opposite compensating charges occur at the Cr_2O_3 surface on positively and negatively poled LiNbO_3 , no significant difference between O atom adsorption on Cr_2O_3 on the two polar substrates or on non-polar $\alpha\text{-Al}_2\text{O}_3$ (0001) could be detected. Further TPD experiments using more sensitive probe molecules, such as alcohols, will be necessary to determine if the substrate polarization has can affect the surface chemical properties of Cr_2O_3 ; since the charge compensation likely occurs at the Cr_2O_3 surface, any effect of the substrate polarization on the surface properties of the Cr_2O_3 is likely to persist for relatively thick films.

6. Acknowledgements

The authors thank Min Li, Boris Lukanov, and Jonathon Huang for their assistance in carrying out this work, and Prof. Victor Henrich for illuminating discussions. This work was supported by the National Science Foundation through grants CHE-1213751 and DMR-1119826

which supports the Center for Research on Interface Structures and Phenomena, the Yale Materials Research Science and Engineering Center.

References

- 1 Y. Yun, M. Li, D. Liao, L. Kampschulte and E.I. Altman, *Surf. Sci.*, 2007, **601**, 4646.
- 2 S.V. Levchenko and A.M. Rappe, *Phys. Rev. Lett.*, 2008, **100**, 256101.
- 3 S. Sanna, S. Rode, R. Hölscher, S. Klassen, C. Marutschke, K. Kobayashi, H. Yamada, W.G. Schmidt and A. Kühnle, *Phys. Rev. B*, 2013, **88**, 115422.
- 4 S.C. Bharath, K.R. Pimputkar, A.M. Pronschinske and T.P. Pearl, *Appl. Surf. Sci.*, 2008, **254**, 2048.
- 5 Y. Yun, L. Kampschulte, M. Li, D. Liao and E.I. Altman, *J. Phys. Chem. C*, 2007, **111**, 13951.
- 6 J. Garra, J.M. Vohs and D.A. Bonnelli, *Surf. Sci.*, 2009, **603**, 1106.
- 7 Zhengzheng Zhang, P. Sharma, C.N. Borca, P.A. Dowben and A. Gruverman, *Appl. Phys. Lett.*, 2010, **97**, 243702.
- 8 S. Habicht, R.J. Nemanich and A. Gruverman, *Nanotechnology*, 2008, **19**, 495303.
- 9 D. Li, M.H. Zhao, J. Garra, A.M. Kolpak, A.M. Rappe, D.A. Bonnelli and J.M. Vohs, *Nature Materials*, 2008, **7**, 473.
- 10 M.H. Zhao, D.A. Bonnelli and J.M. Vohs, *Surf. Sci.*, 2008, **602**, 2849.
- 11 J.L. Giocondi and G.S. Rohrer, *Chem. Mater.*, 2001, **13**, 241.
- 12 M.W. Herdiech, H. Mönig and E.I. Altman, *Surf. Sci.*, 2014, **626**, 53.
- 13 C. Noguera, *J. Phys.-Condens. Mat.*, 2000, **12**, 367.
- 14 Y. Inoue, Y. Imai and K. Sato, *Chem. Phys. Lett.*, 1989, **160**, 118.
- 15 Y. Inoue, K. Sato and S. Suzuki, *J. Phys. Chem.*, 1985, **89**, 2827.
- 16 Y. Inoue, I. Yoshioka and K. Sato, *J. Phys. Chem.*, 1984, **88**, 1148.
- 17 A.M. Kolpak, I. Grinberg and A.M. Rappe, *Phys. Rev. Lett.*, 2007, **98**, 166101.
- 18 Y. Yun, N. Pilet, U.D. Schwarz and E.I. Altman, *Surf. Sci.*, 2009, **603**, 3145.
- 19 L.E. Briand, W.E. Farneth and I.E. Wachs, *Catal. Today*, 2000, **62**, 219.
- 20 M.H. Zhao, D.A. Bonnelli and J.M. Vohs, *J. Vac. Sci. Technol. A*, 2009, **27**, 1337.
- 21 S. Kim, M.R. Schoenberg and A.M. Rappe, *Phys. Rev. Lett.*, 2011, **107**, 076102.
- 22 M.P. McDaniel, *J. Catal.*, 1982, **76**, 17.
- 23 M.P. McDaniel, *J. Catal.* 1982, **76**, 29.
- 24 R. Merryfield, M. McDaniel and G. Parks, *J. Catal.*, 1982, **77**, 348.
- 25 D. Sanfilippo, F. Buonomo, G. Fusco, M. Lupieri and I. Miracca, *Chem. Eng. Sci.*, 1992, **47**, 2313.
- 26 D.S. Kim and I.E. Wachs, *J. Catal.*, 1993, **142**, 166.
- 27 R.S. Weis and T.K. Gaylord, *Appl. Phys. A*, 1985, **37**, 191.
- 28 W.Y. Ching, Z.-Q. Gu and Y.-N. Xu, *Phys. Rev. B*, 1994, **50**, 1992.
- 29 H.D. Megaw, *Acta Cryst.*, 1954, **7**, 187.
- 30 W. Gao, C.M. Wang, H.Q. Wang, V.E. Henrich and E.I. Altman, *Surf. Sci.*, 2004, **559**, 201.
- 31 C.A.F. Vaz, D. Prabhakaran, E.I. Altman and V.E. Henrich, *Phys. Rev. B*, 2009, **80**, 155457.
- 32 S.-Y. Jeong, J.-B. Lee, H. Na and T.-Y. Seong, *Thin Solid Films*, 2010, **518**, 4813.
- 33 S.A. Chambers, *Surf. Sci. Rep.*, 2000, **39**, 105.
- 34 S.A. Chambers, Y. Liang and Y. Gao, *Phys. Rev. B*, 2000, **61**, 13223.
- 35 J.D.J. Ingle, S.R. Crouch, *Spectrochemical Analysis*, Prentice Hall, New Jersey, 1988.
- 36 M.P. Seah and W.A. Dench, *Surf. Interface Anal.*, 1979, **1**, 2.

- 37 F. Caccavale, in 'Properties of LiNbO₃,' ed. K.K. Wong, Institute of Engineering and Technology, London, 2002.
- 38 G.M. Salley, S.A. Basun, G.F. Imbusch, A.A. Kaplyanskii, S. Kapphan, R.S. Meltzer and U. Happek, *J. Lumin.*, 1999, **83-84**, 423.
- 39 S. Veliah, K.-H. Xiang, R. Pandey, J.M. Recio and J.M. Newsam, *J. Phys. Chem. B*, 1998, **102**, 1126.
- 40 I. Ikemoto, K. Ishii, S. Kinoshita, H. Kuroda, M.A. Alario Franco and J.M. Thomas, *J. Solid State Chem.*, 1976, **17**, 425.
- 41 H. A. Bullen and S.J. Garrett, *Chem. Mater.*, 2002, **14**, 243.
- 42 G.C. Allen, M.T. Curtis, A.J. Hooper and P.M. Tucker, *J. Chem. Soc., Dalton Trans.*, 1973, **16**, 1675.
- 43 J.F. Moulder, W.F. Stickle, P.E. Sobol, K.D. Bomben, *Handbook of X-ray Photoelectron Spectroscopy*, Perkin-Elmer, 1992.
- 44 B. Liu and M. Terano, *J. Mol. Catal. A*, 2001, **172**, 227.
- 45 F. Cavani, M. Koutyrev, F. Trifirò, A. Bartolini, D. Ghisletti, R. Iezzi, A. Santucci and G. Del Piero, *J. Catal.*, 1996, **158**, 236.
- 46 V. Gopalan, T.E. Mitchell, Y. Furukawa and K. Kitamura, *Appl. Phys. Lett.*, 1998, **72**, 1981.
- 47 A. Mansingh and A. Dhar, *J. Phys. D: Appl. Phys.*, 1985, **18**, 2059.
- 48 J.A. Geuther and Y. Danon, *J. Appl. Phys.*, 2005, **97**, 074109.
- 49 J.D. Brownridge, *Nature*, 1992, **358**, 287.
- 50 B. Naranjo, J.K. Gimzewski and S. Putterman, *Nature*, 2005, **434**, 1115.
- 51 A. Savage, *J. Appl. Phys.*, 1966, **37**, 3071.
- 52 J.D. Brownridge, S.M. Shafroth, Electron and Positive Ion Beams and X-rays Produced by Heated and Cooled Pyroelectric Crystals such as LiNbO₃ and LiTaO₃ in Dilute Gases: Phenomenology and Applications, in: W.T. Arkin (Ed.) Trends in Lasers and Electro-Optics Research, Nova Science Publishers, 2006, pp. 59-95.
- 53 L.E. Klebanoff, S.W. Robey, G. Liu and D.A. Shirley, *Phys. Rev. B*, 1984, **30**, 1048.
- 54 D. Tobia, E. Winkler, R.D. Zysler, M. Granada and H.E. Troiani, *Phys. Rev. B*, 2008, **78**, 104412.
- 55 Ö. Özdemir and D.J. Dunlop, *Geophys. Res. Lett.*, 1993, **20**, 1671.
- 56 J.P. Wright, A.M.T. Bell and J.P. Attfield, *Solid State Sci.*, 2000, **2**, 747.
- 57 J.P. Wright, J.P. Attfield and P.G. Radaelli, *Phys. Rev. B*, 2002, **66**, 214422.
- 58 B.M. Weckhuysen, L.M. De Ridder and R.A. Schoonheydt, *J. Phys. Chem.*, 1993, **97**, 4756.
- 59 S.C. York, M.W. Abee and D.F. Cox, *Surf. Sci.*, 1999, **437**, 386.
- 60 W.-C. Wang, B.J. Rodriguez, A. Gruverman and R.J. Nemanich, *J. Phys.: Condens. Matter*, 2005, **17**, S1415.
- 61 E.A. Kraut, R.W. Grant, J.R. Waldrop and S.P. Kowalczyk, *Phys. Rev. Lett.*, 1979, **44**, 1620.

Figure Captions

Figure 1: Ball and stick model showing a (a) side view and (b) top view of an ideal epitaxial Cr_2O_3 epitaxial thin film on LiNbO_3 (0001). The red balls represent O atoms, the blue Nb, the green Li, and the gray Cr. The model does not include any potential surface and interfacial reconstructions and the Cr_2O_3 is compressed in-plane to match the LiNbO_3 a lattice parameter. The spacings provided in (a) are for the bulk materials.

Figure 2: X-ray diffraction data for a 14 nm (\approx 60 ML) Cr_2O_3 film on positively poled LiNbO_3 (0001): (a) θ - 2θ scan showing the LiNbO_3 (006) and Cr_2O_3 (006) region; and (b) expanded view of the XRR fringes. Samples were annealed in ambient pressure O_2 for 30 min unless otherwise noted. Cr_2O_3 was deposited at 575 K.

Figure 3: Normalized Cr 2p and Nb 3d XPS peak area versus Cr_2O_3 film thickness for Cr_2O_3 on (a) positively and (b) negatively poled LiNbO_3 . The solid lines highlight the expected growth and decay of the Cr 2p and Nb 3d peaks, respectively. The calculations are based on a 12.5 Å mean free path for the Cr 2p emission and 15.2 Å for emission from Nb 3d levels.

Figure 4: RHEED patterns for (a) 0 ML, (b) 1 ML, (c) 2 ML, (d) 4 ML, and (e) 6 ML Cr_2O_3 on negatively poled LiNbO_3 . The data were collected at an electron energy of 15 keV with the beam parallel to the LiNbO_3 [1000] direction.

Figure 5: LEED patterns for: (a) 1.0 ML, (b) 8.6 ML, and (c) 10.1 ML Cr_2O_3 on negatively poled LiNbO_3 .

Figure 6: LEED patterns for: (a) 12 nm (\approx 55 ML) Cr_2O_3 on α - Al_2O_3 (0001), (b) 20 nm (\approx 90 ML) Cr_2O_3 on positively poled LiNbO_3 (0001), and (c) 20 nm (\approx 90 ML) Cr_2O_3 on negatively poled LiNbO_3 (0001) after annealing in air for 12 h at 875 K.

Figure 7: Comparison of (a) Cr 2p and (b) Nb 3d XPS peaks before and after a 12 hr anneal in atmospheric pressure air at 875 K for a 10.0 ML Cr_2O_3 film on positively poled LiNbO_3 (0001).

Figure 8: XPS Cr 2p peaks for increasingly thick Cr_2O_3 films on (a) positively and (b) negatively poled LiNbO_3 .

Figure 9: Cr $2p_{3/2}$ XPS peak positions as a function of temperature for 3 ML Cr_2O_3 films on (a) positively and (b) negatively poled LiNbO_3 (0001).

Figure 10: Cr 2p XPS peaks for (I) as grown Cr_2O_3 and (II) after exposing surfaces to oxygen plasma at room temperature for Cr_2O_3 on (a) positively and (b) negatively poled LiNbO_3 (0001).

Figure 11: LEED patterns for 2.0 ML Cr_2O_3 on positively poled LiNbO_3 (0001) (a) before and (b) after exposure to oxygen plasma at room temperature.

Figure 12: Cr 2p XPS peaks as a function of temperature after exposure to reactive species emitted from the oxygen plasma at room temperature for (a) 1.6 ML Cr₂O₃ on positively poled LiNbO₃ (0001), (b) 3.1 ML Cr₂O₃ on negatively poled LiNbO₃ (0001), (c) 6.0 ML Cr₂O₃ on positively poled LiNbO₃ (0001), and (d) 12 nm (\approx 55 ML) Cr₂O₃ on α -Al₂O₃ (0001).

Figure 13: Oxygen TPD trace obtained after exposing a 12 nm (\approx 55 ML) Cr₂O₃ film on α -Al₂O₃ (0001) to the plume of the oxygen plasma source.

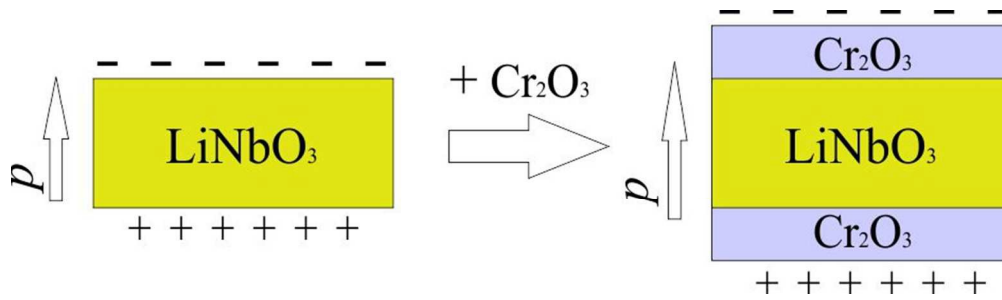


Illustration showing non-polar Cr_2O_3 deposition onto ferroelectric LiNbO_3 . Characterization of the interface suggests that the charge compensation layer migrates to the chromium oxide surface where it can lead to distinct chemistry on oppositely poled substrates.

80x22mm (300 x 300 DPI)